ADVANCED FUNCTIONAL MATERIALS
www.afm-journal.de

Multifurcate Assembly of Slanted Micropillars Fabricated by Superposition of Optical Vortices and Application in High-Efficiency Trapping Microparticles

Jincheng Ni, Zhongyu Wang, Ziqin Li, Zhaoxin Lao, Yanlei Hu, Shengyun Ji, Bing Xu, Chenchu Zhang, Jiawen Li,* Dong Wu,* and Jiaru Chu*

Self-assembly induced by capillary force is abundant in nature and has been widely used in fabrication as a bottom-up method. Here a rapid and flexible method for achieving an even number of furcate slanted micropillars by single-exposure under a spatial phase modulated laser beam is reported, which is produced by designing a superimposed hologram with opposite topological charges to split the incident beam into several equal-weighting sectors. These furcate micropillars with intentional spatial arrangement can be directed to capillary-assisted self-assembly process for generating designable hierarchical functional arrays. Due to the slanted characteristic of micropillars (8°–13°), the assembled arrays are very stable and can be used as an effective tool for trapping SiO_2 particles to form honeycomb patterns with an ultrahigh trapping ratio (>90%), which can image as a microlens array. The investigation reveals that micropillars with a height of 6 µm exhibit the high trapping ratio of particles, which maintain a fine imaging performance. The fast fabrication (more than 2 orders of magnitude enhancement) of furcate slanted pillars paves an avenue for developing innovative microoptics, microfluidics and biological scaffold engineering.

1. Introduction

Self-assembly of filaments induced by capillary force is ubiquitous in nature, such as seaweed or wet hair pulling out of water. Capillary force can also drive the adhesion of straight high-aspect-ratio micro/nanopillars, which is an undesirable but inevitable phenomenon for researching artificial biomimetic surfaces,[1] bioinspired reversible interlocker,[2] and nanofiber-based sensors.[3] Meanwhile, there are many attempts to analyze the assembled mechanism and control the collapse to build designed structures. For example, the high-aspect-ratio micro/nanostructures can be directionally collapsed to form designed patterns by controlling their cross-sections, heights, distances, and tilted angles.[4–7] Up until now, many fabrication approaches have been utilized together with capillary driven self-assembly to create functional microstructures, including electron-beam lithography,[4] deep dry etching,[6] direct laser writing,[5,8] multibeam laser interference,[9] and replica molding.[10] Among them, femtosecond direct laser writing is a promising method with advantages of high resolution, good scalability, and high controllability. However, femtosecond laser needs to fabricate the high-aspect-ratio micro/nanopillars with single-spot scanning, resulting in a low fabrication efficiency. According to the previous studies, a variety of methods, such as microlens arrays,[11] spatial light modulator (SLM),[12] and multibeam interference with four-titled plane waves[13] have been developed for rapid laser fabrication, but these methods have not yet been explored for fabricating furcate pillars. In addition, the assembled micropillars have received much attention recently because their ability in trapping microobjects is potentially used in the fields of biomedical devices and chemical analysis.[6,9,14] However, one challenge of these applications is the relatively low trapping ratio (<40%) because only a part of the straight micro/nanopillars which are used as grippers can catch particles successfully when capillary force driving the pillars to self-assembly. After immersed in liquid again, the trapped particles can escape because the assembled pillars return to standing state and the grippers are open. Therefore, rapid fabrication of micropillars for self-assembled microstructures with an ultrahigh trapping ratio is highly desired.

Optical vortices, which carry orbital angular momentum (OAM) of $l\hbar$ (l is an integer, called topological charge and $\hbar$ is reduced Planck's constant), have helical phase wavefronts and "doughnut"-shaped intensity profiles. The vortex beam has been comprehensively used in optical tweezers,[15] optical communications,[16] detecting spinning objects,[17] and fabricating chiral microstructures.[18] The superposition of opposite optical vortices with topological charges $\pm l$ has been proved to be able to generate $2l$ bright dots in a "doughnut"-shaped distribution.[19] Yet, to date, the fabrication of controllable micro/nanostructures or functional devices with superposition of the opposite optical vortices has remained unseen.

J. Ni, Z. Wang, Z. Li, Z. Lao, Dr. Y. Hu, S. Ji, B. Xu, Dr. C. Zhang, Dr. J. Li, Prof. D. Wu, Prof. J. Chu
CAS Key Laboratory of Mechanical Behavior and Design of Materials
Department of Precision Machinery and Precision Instrumentation
University of Science and Technology of China
Hefei, Anhui 230027, China
E-mail: huyl@ustc.edu.cn; jwl@ustc.edu.cn; dongwu@ustc.edu.cn

DOI: 10.1002/adfm.201701939

Here, we report a flexible and rapid strategy for achieving an even number ($2l$) of furcate slanted micropillars by a single exposure of spatial phase modulated laser beam. An incident Gaussian beam is divided into $2l$ sectors for forming multiple spots intensity distributions by a superimposed hologram with opposite topological charges. The fabrication efficiency can increase 2 orders of magnitude compared with traditional direct laser writing. These furcate micropillars with intentional spatial arrangement can be directed to self-assembly process for generating designable hierarchical array, which is stable due to the slanted pillars. Moreover, this assembled array is used as an effective tool for trapping particles with an ultrahigh trapping ratio (>90%) to form a honeycomb pattern, which can image as a microlens array.

2. Results and Discussion

2.1. High-Efficiency Holographic Fabrication of Multifurcate Slanted Micropillars by Modulating Optical Field with an SLM

The main concept for fabricating multifurcate micropillars in our experiment is schematically illustrated in **Figure 1**a. A collimated linearly polarized femtosecond laser beam with a central wavelength of 800 nm is modulated into six beamlets by a hologram with topological charge $l = \pm 3$ displayed on an SLM. A tilted shift phase hologram is added to the opposite OAM hologram for separating the first-order diffracted beam. A $4f$ relay system with an iris located at the focal plane of a lens L_1 is used for filtering the undesired order of diffraction (Figure S1, Supporting Information). This modulated beam is focused to generate diverging multipoint optical field along z axis by a 60× oil-immersion objective lens (NA 1.35), as shown in Figure 1b. The multipoint femtosecond laser is used to generate six furcate slanted micropillars with circular cross-section in a photoresist sample, by means of precisely controlling the laser power and exposure time (see the Experimental Section for details). The inverted sample is mounted on a nanopositioning stage to precisely locate microstructures with nanometer resolution. Six-furcate slanted micropillars are obtained in the sample after the unpolymerized part is washed away, as illustrated in Figure 1c.

2.2. Optical Intensity Distributions and Corresponding Microstructures Produced by Holograms with Various Topological Charges

Laguerre–Gaussian beam with opposite topological charge $l = \pm 3$ produces six lattice sites and an alternative phase value distribution (Figure 1d–f). The optical interference of opposite optical vortices has bright dots in a "doughnut"-shaped distribution and quantized phase at either 0 or π corresponding to intensity maxima and minima, which can also be found in a whispering gallery mode resonator.[20] The holograms for generating interference of opposite optical vortices with topological charge $\pm l$ can be presented as

$$\varnothing(r,\varphi) = \exp(il\varphi) + \exp(-il\varphi) \tag{1}$$

where φ is the azimuthal coordinate (**Figure 2**a–c). Two counter-helical phase wavefronts interfere to form an interference pattern with a transverse intensity profile comprising of $2l$ bright or dark petals. The simulated optical intensity can be derived by the vectorial Debye diffraction theory for the high numerical aperture objective (see the Experimental Section). Figure 2d–i shows the simulated and measured intensity profiles with different holograms of opposite topological charge $l = \pm 1$, ± 2, ± 3 on the focal plane of objective lens. It can be seen that the modulated beam is focused into the designed intensity pattern comprising of $2l$ petals with a cylindrically symmetric arrangement. After exposed by the laser beam (topological charges $l = \pm 1$) without time-consuming scanning, double furcate slanted pillars with a tilted angle of $\beta = 8°$ are polymerized in the sample (Figure S2, Supporting Information). The exposure time is 1 s and the laser power is 20 mW measured before injecting in the microscope system (Figure 2j). The exposure laser power is 30 and 40 mW for fabricating slanted four- and six-pillars ($\beta = 11°$ and 13°), respectively (Figure 2k,l). As the laser power increases to 100 mW, the secondary pillars are fabricated adjacently to the four-furcate micropillars (Figures S3 and S4, Supporting Information). The exposure time of 20 ms for fabricating single six-micropillar unit with the laser power of 100 mW is much shorter than that of 3.6 s by conventional point-to-point scanning (Videos S1 and S2, Figure S5, Supporting Information). Large-area assembled microstructures (1 mm^2) can be realized with the fabrication time of less than 5 min.

2.3. Capillary Force Induced Controllable Self-Assembly of Multifurcate Slanted Pillars with Different Intervals

Individual vertical pillars can be bent and stuck to adjacent ones at their top ends with the aid of evaporation-induced capillary force.[5] This phenomenon can also be found in multifurcate slanted pillars fabricated by superposition of opposite optical vortices. As a double-pillars unit is diverged, the distance between its two tips is larger than the bottom distance. As a result, it can be visualized from the scanning electron microscope (SEM) images that capillary force bends the furcate pillars to almost vertical situation but hardly contacting each other (Figure 2j–l). In order to realize self-assembly, we can control the distance between adjacent micropillar units by moving the nanopositioning stage in the horizontal directions. The self-assembly process between the furcate pillars can be considered as a competition between elastic restoring forces and evaporation-induced capillary forces, as shown in **Figure 3**a. As developed liquid evaporates to the tips of tilted pillars, a menisci interface between the tips will produce a capillary force presented as[5,21]

$$F_c \sim \gamma r^2 \cos^2\theta / (\Delta d - d) \tag{2}$$

where γ, r, θ, Δd, and d are surface tension, the radius of pillars, contact angle, the interval between adjacent pillars units and the distance between symmetric tips in a unit, respectively. There is also a supporting force to resist the capillary force, generating by an elastic restoring force, which can be defined as[7]

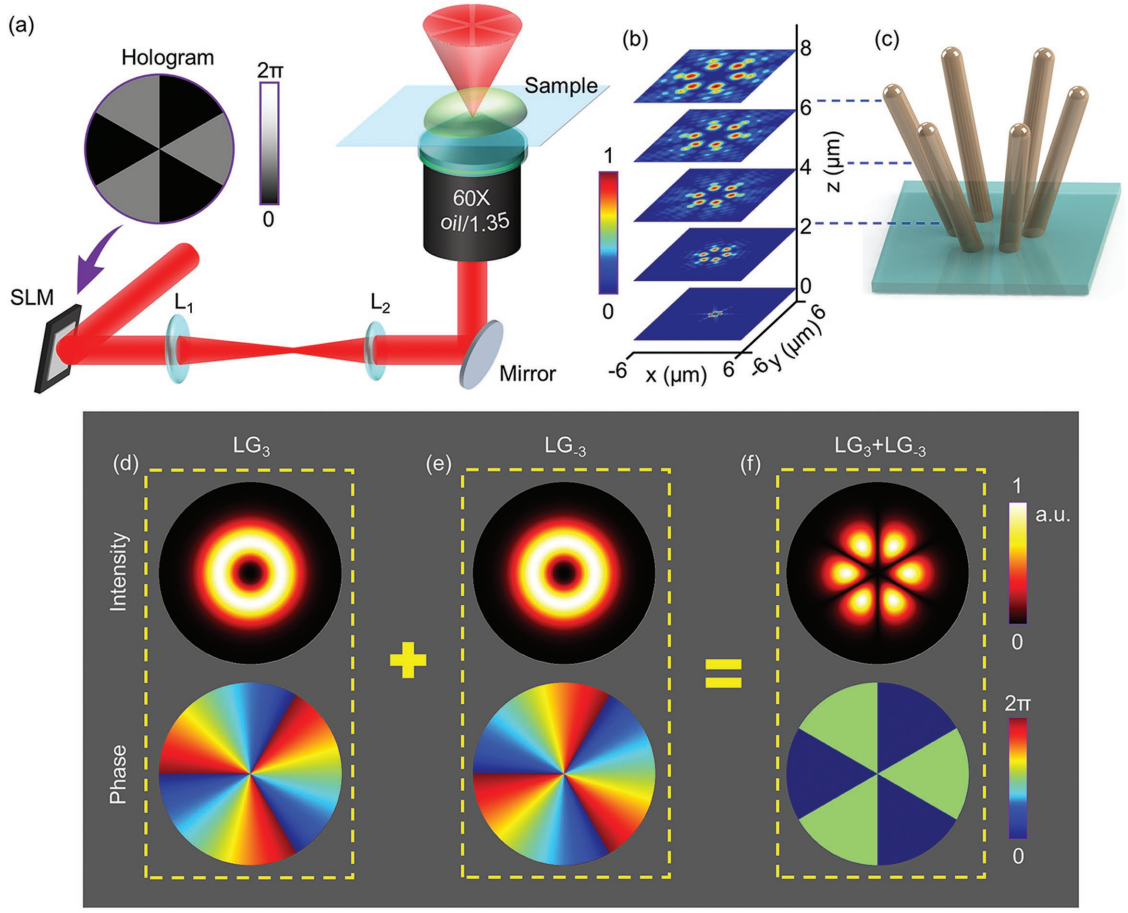

Figure 1. High-efficiency holographic fabrication of six furcate slanted micropillars by modulating optical field with an SLM. a) SLM-based optical setup for fabrication. The femtosecond laser is modulated to six beamlets by an SLM, which displays the designed hologram. b) The simulated optical intensity distribution of superposition of opposite optical vortices under the objective lens at different *z* planes. c) Illustration of six-furcate micropillars is polymerized in the sample illuminated by opposite optical vortices without scanning procedure. The simulated intensity and phase distribution of optical vortex with topological charge of d) $l = 3$ and e) $l = -3$. f) Bright optical lattices are obtained by the interference of optical vortices with opposite topological charge $l = \pm 3$.

$$F_s \sim Er^4\delta/(h/\cos\beta)^3 \quad (3)$$

where E, δ, h, and β are Young's modulus, the deflection of pillar from original location, the height, and the tilted angle of pillars, respectively. According to the formulas, a small interval between the tips and a large height of pillars ($F_s < F_c$) facilitate self-assembly process. The double-micropillars in a row are isolated with a sparse interval ($\Delta d \geq 5$ μm), where capillary force is not strong enough to bend the pillars to contact each other (Figure 3b). When the double-micropillars are arranged with a moderate interval ($4 < \Delta d \leq 5$ μm), they are assembled by capillary force after liquid solvents evaporation (Figure 3c). Once the distance decreases to a tight interval ($\Delta d \leq 4$ μm), the pillars connect each other by polymerization instead of self-assembly process, as shown in Figure 3d. To systematically study the different states of micropillars (isolation, self-assembly, or polymerization), parameter studies are performed by fabricating a series of pillar arrays with different intervals and heights. It is important to note that the intervals between micropillars units predominate the result of evaporation in our experiment, as shown in Figure 3e. Owing to the high flexibility of laser-modulated technique, more even numbers of micropillars can be achieved by loading diverse holograms on the SLM. The assemblies of adjacent units can also be found in four- and six-pillars array by controlling their positions on the substrate. For realizing equal intervals between corresponding slanted micropillars, four- and six-furcate pillars are arranged in square and triangular patterns, respectively (Figure 3f,i). When keeping a sparse interval for four-(10 μm) and six-(15 μm) pillar array, the furcate pillars remain standing after liquid evaporation process (Figure 3g,j). By precisely tuning the intervals between the units, four- and six-pillars assembled array are achieved. Due to the excellent control of spatial phase modulated laser, fine replication of furcate four-/six-pillars and high uniformity of self-assembly property can be realized (Figure 3h,k). More asymmetric patterns can also be realized by controlling the furcate micropillars and their arrangements on the substrate (Figure S6, Supporting Information). The assembled arrays of furcate slanted pillars are stable after immersed in solvent again, while straight pillars return to standing state.[9]

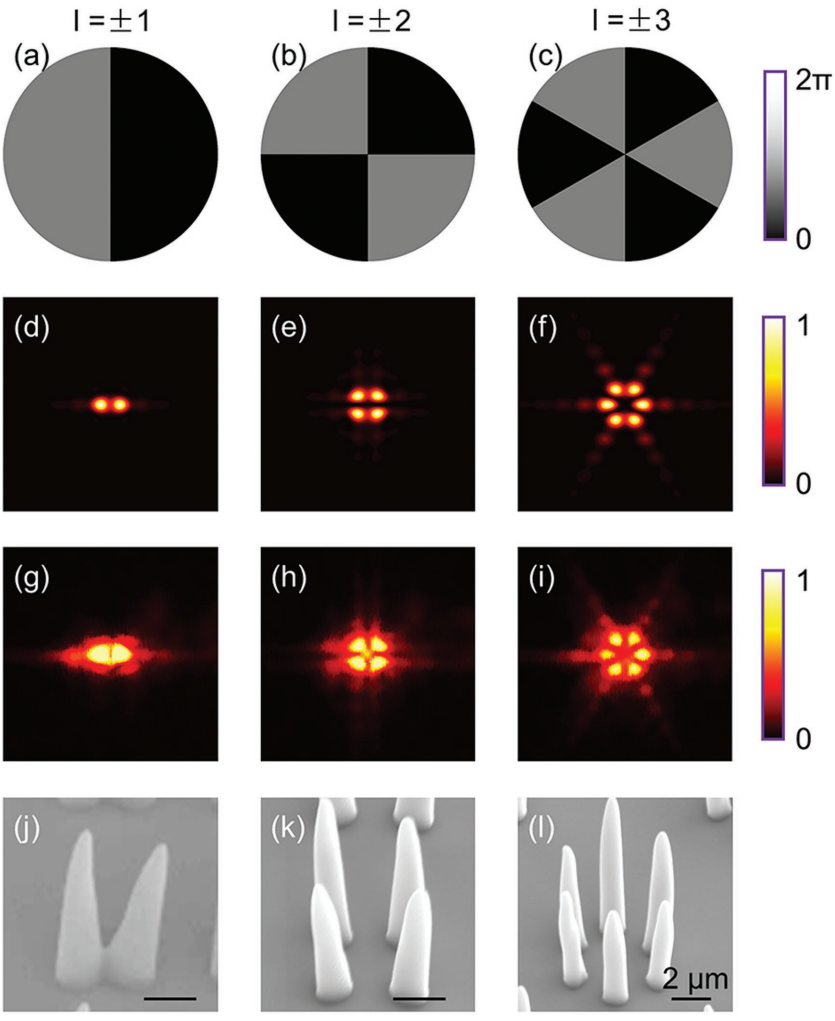

Figure 2. Flexible control of optical intensity distributions and corresponding microstructures by laser-modulated beam with various topological charges. Holograms for generating interference beams with superimposed holograms with topological charge a) $l = \pm 1$, b) $l = \pm 2$, and c) $l = \pm 3$. d–f) Simulated and g–i) measured optical intensity patterns on the focal plane of an oil-immersion objective lens with NA = 1.35 corresponding to the holograms in (a–c). After developing, 45° tilted-view SEM images j–l) of two-, four-, and six-furcate slanted micropillars with the original angles of 8°, 11°, and 13°. The fabrication efficiency can be enhanced by 2 orders of magnitude compared with traditional direct laser writing.

2.4. Microscale Topographic Control of Capillary Assembly for Trapping Microobjects

The ability of manipulating particles desired in biological devices and chemical analysis has drawn crucial attentions from researchers.[14] For example, substantial mechanical grippers are used to capture, hold, and analyze living cells for genomics, proteomics, and diagnostics.[22] Moreover, nanofingers can capture analyte molecules on their tips by capillary-force-driven self-assembly to form a Raman hot spot for molecule detection and identification based on surface enhanced Raman spectroscopy (SERS).[23] Here, we demonstrate that the assembled micropillars array in our experiment can be harnessed for trapping particles, as illustrated in **Figure 4**a. In the procedure, distilled water solution containing 5 μm diameter SiO_2 particles is dropped on the horizontal sample with assembled pillars array (see the Experimental Section). A part of particles are trapped within microcavities of assembled-pillars units modulated by gravity and hydrodynamic forces. Then the sample is washed in distilled water for flushing away the non-captured particles. These assembled-pillars maintain contacting with each other in water because the elastic restoring force of tilted pillars is smaller than van der Waals' force (Figure S12, Supporting Information). The trapped particles with a grasping force produced by contacting pillars are relatively more stable than free-particles. So the trapped particles are increased with repeating cycles, as shown in Figure 4b,c. In the end, almost all microcavities are filled with particles after repeating this process about four times. These particles are arranged in a honeycomb shape by trapping in the center of six-micropillar units (Figure 4d,e). As the furcate micropillars are fabricated by the spatial-modulated optical field, the gaps between trapped particles and high ($h \geq 6$ μm)/short ($h = 4$ μm) pillars are located at the bottom/flank of particles (Figure 4f). When the height of pillars is $h = 4$ μm, the trapped particles in microcavities are not stable enough to survive in the washing process because of the less contact area between micropillars and particles. We investigate that trapping ratio of microcavities, which is assembled by high pillars ($h = 6$ μm), is increasing with repeating cycles (Figure 4g). As a result, 4 μm height pillars relatively trap less particles (≈50%) because some trapped particles escape from the microcavities, as shown in Figure 4h. According to our experiments, the trapping efficiency can reach to >90% and can be further improved by repeating the trapping process (Figures S7 and S8, Supporting Information). However, in the previous reports,[5,9] the trapping efficiency of straight pillars array is <40% because the assembled pillars recover after being immersed in solvent.

The trapped particles are stable in the iterative process because of the strong van der Waals force between pillars and particles. The furcate micropillars are firstly self-assembled to form periodic microcavities in air (**Figure 5**a). When dropping the distilled water solvent containing SiO_2 particles, the trapped particles are fixed in the microcavities by balancing the acting forces-gravity (F_g), buoyancy (F_f), supporting force (F_s), and van der Waals force (F_{v1}), as shown in Figure 5b. To analyze magnitude of the relative force, we reverse the sample to remove the supporting force (Figure 5c). The trapped particles maintain stable in the microcavities after evaporation process, which means that the van der Waals force is larger than gravity of particles (Figure 5d). The van der Waals force determined by gravity and the tilted angle of pillars is presented as

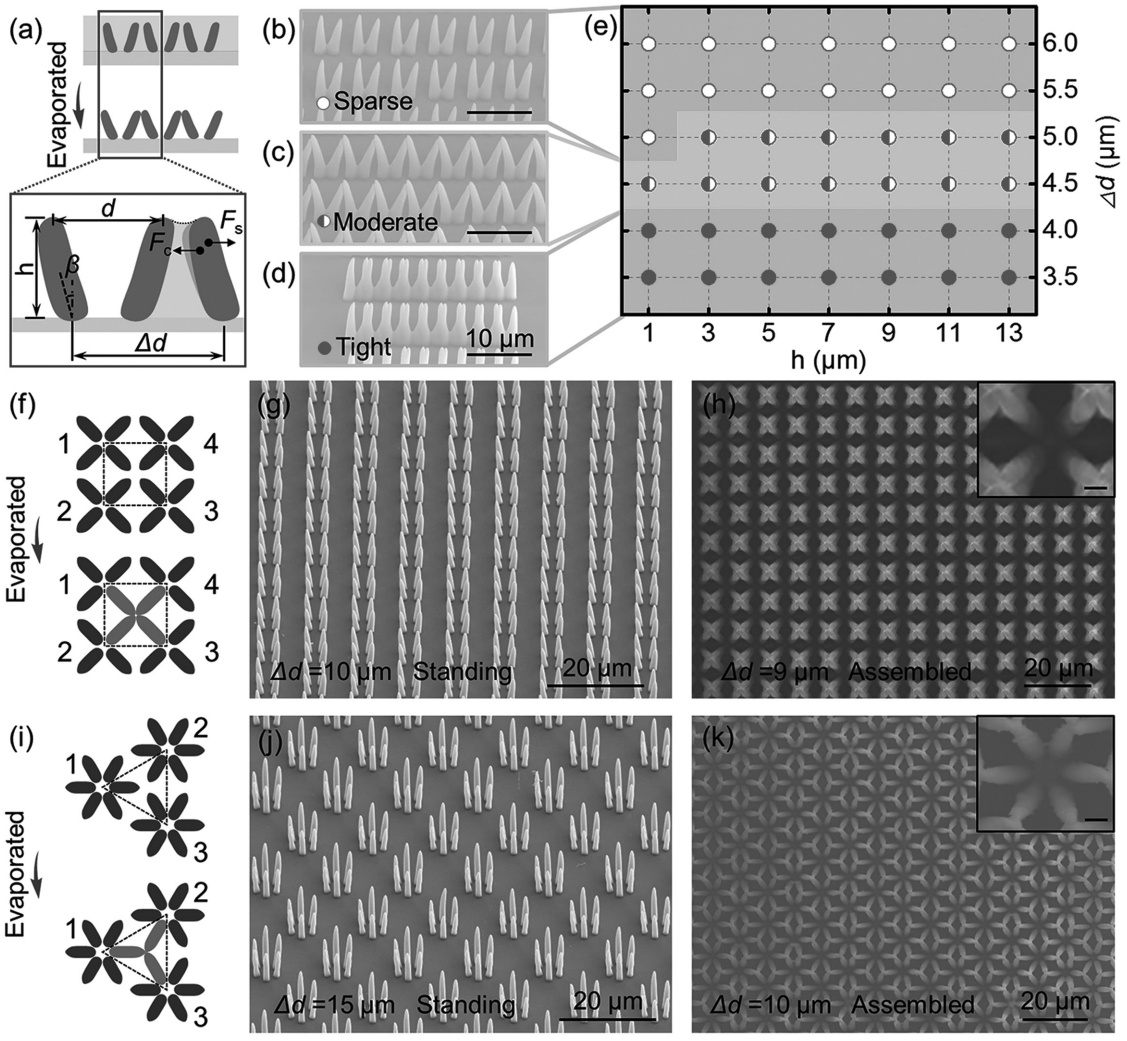

Figure 3. Capillary force induced controllable self-assembly of multifurcate (2, 4, and 6) slanted micropillars with different intervals. a) Illustration of the self-assembly process between adjacent furcate pillars with a moderate interval and forces acting on the pillars during evaporation process. Tilted SEM images of double-furcate micropillars fabricated in alignment with a b) sparse, c) moderate, and d) tight interval. e) The quantitative study is conducted on the intervals and heights of double micropillars with different states after evaporation. f) Top-viewed schematic of four micropillars with square arrangement and the self-assembly result. Black dashed lines indicate the moderate intervals (Δd) between four adjacent micropillars units. Four furcate pillars in the dashed box are bent and stuck at their tips with the aid of evaporation-induced capillary force. g) Tilted SEM image of a four-micropillar array with a sparse interval. h) Top-view SEM image of a four-micropillar array with a moderate interval. i) Corresponding schematic as in (f), for the case of six micropillars with triangular arrangement. Six-micropillar array with a j) sparse and k) moderate interval. Insets are the magnified views (scale bar, 2 μm).

$$F_{v3} = \frac{F_g}{6\sin\beta} \quad (4)$$

There are no particles falling out when we inverse the sample with trapped particles (Figure 5e,f). In fact, the trapped particles can still be trapped even if the sample is flushed under distilled water (Video S3, Supporting Information).

2.5. Imaging Test of the Sample after Trapping SiO_2 Particles

Microscale and nanoscale functional devices constituted by the complex nested microlens array can be used as a relief mask for generating diffraction images like a kaleidoscope[24] and integrated on optical fiber tips for sensing applications.[25] Here the trapped particles in microcavities of furcate slanted micropillars can be used for imaging periodic patterns. An optical setup for imaging test of sample is shown in **Figure 6**a. The intensity distribution on the focal plane of trapped particles can be caught by a charge-coupled device (CCD) (see the Experimental Section). It is indicated that the focusing performance of particles is related with the height of pillars (Figure 6b, Figures S9 and S10, Supporting Information). As the roots of high tilted pillars are under the trapped particles, these parts projecting on the microsphere will affect the imaging performance, which is simulated using Comsol Multiphysics 5.2 (Figure S11, Supporting Information). Consequently, the optical intensity of focusing spot decreases with

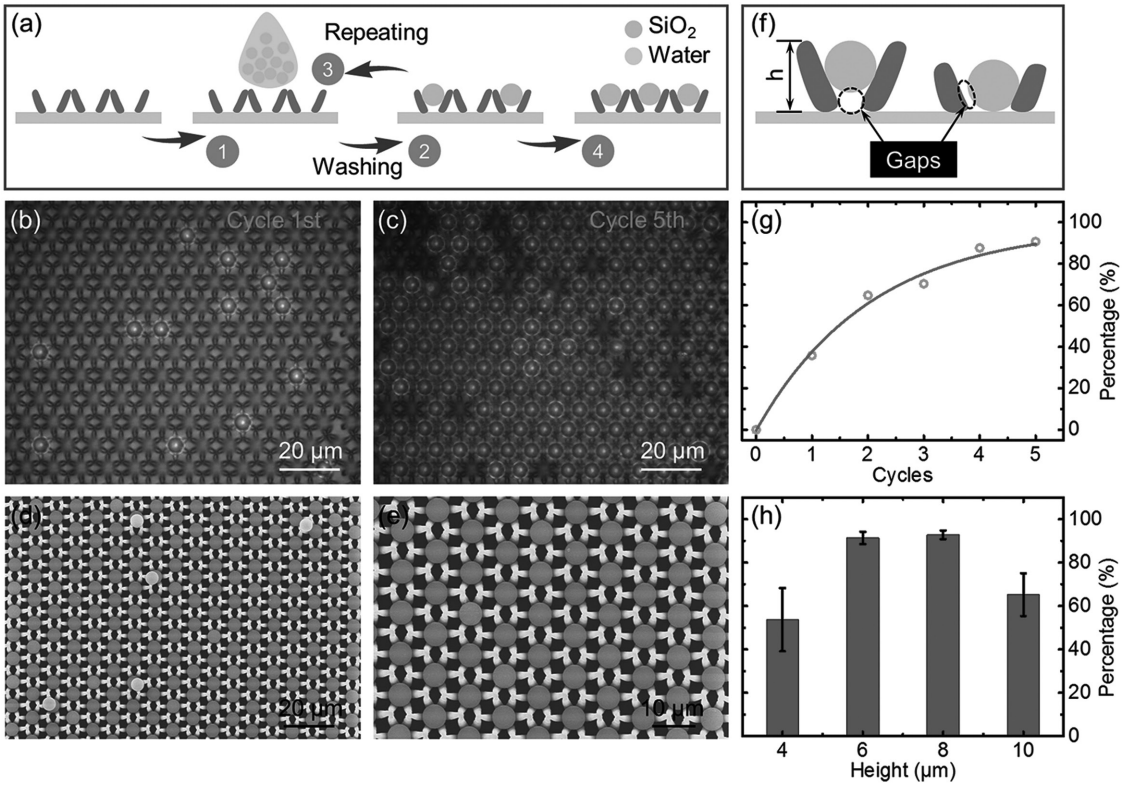

Figure 4. Microscale topographic control of capillary assembly for trapping particles with ultrahigh ratio (>90%). a) Schematic of the SiO_2 particles traps of the six-micropillar array (dimensions not to scale). The distilled water solution mixed with SiO_2 particles is dropped on the sample after self-assembly process. Then the sample is flushed by distilled water to wash away the free particles. A high trapping ratio is achieved after iterating this process. Optical images of the sample are captured after washing for cycle once (b) and fifth (c). d) SEM image of the sample after trapping SiO_2 particles. e) A magnified view. f) Schematic of trapping SiO_2 particles with different height of six micropillars. g) Quantitative study on the percentage of trapping ratio as a function of cycles (h = 6 μm). The curve is drawn as a guide to the eye. h) Trapping ratio of the sample as a function of the height after iterating over the trapping process for the fifth time. Error bars are the standard deviation of three samples with the same parameters.

increasing the height of furcate slanted pillars. Accordingly, the kaleidoscopic images of a letter "A" by particles with different heights of pillars are achieved by accurately trapping and rearranging particles. The periodic patterns have fine qualities with short pillars (h = 4 and 6 μm), and the qualities become inferior with increasing heights of pillars, shown in Figure 6c–f. Due to the stable capillary-driven self-assembly between furcate slanted micropillars units, the trapped particles located on the same horizontal plane maintain consistent imaging performance.

3. Conclusion

In summary, a rapid and flexible method is proposed to fabricate furcate slanted micropillars with the aid of holographic superposition of opposite optical vortices. The fabrication efficiency of this laser-modulated technique can increase 2 orders of magnitude compared with traditional direct laser writing. These furcate pillars can be accurately self-assembled by controlling their intervals with intentional spatial arrangement. Moreover, the assembled array can trap SiO_2 particles with a high trapping ratio (>90%) to arrange in a honeycomb lattice. The superior imaging quality of trapped particles can be achieved by decreasing the height of pillars. Our investigation reveals that the 6 μm height furcate slanted micropillar arrays have a high trapping ratio and still maintain a fine imaging performance. We believe that the strategy, which combines superimposing optical vortices with capillary-driven self-assembly to rapidly fabricate furcate slanted micropillars, will find extensive applications in microoptics, microfluidics, and biological scaffold engineering.

4. Experimental Section

Numerical Simulation of Field Distribution under the Objective: Considering the linearly polarized laser beam focused by a high NA objective lens after modulated by SLM, the vectorial Debye diffraction theory was used to simulate electromagnetic wave propagation near the focal spot.[26]

Materials and Equipment: A commercially available zirconium-silicon hybrid sol–gel material (SZ2080, IESL-FORTH, Greece) was used for photopolymerization in our experiment. A prebaking process for evaporating the solvent in SZ2080 was set to 45 min on

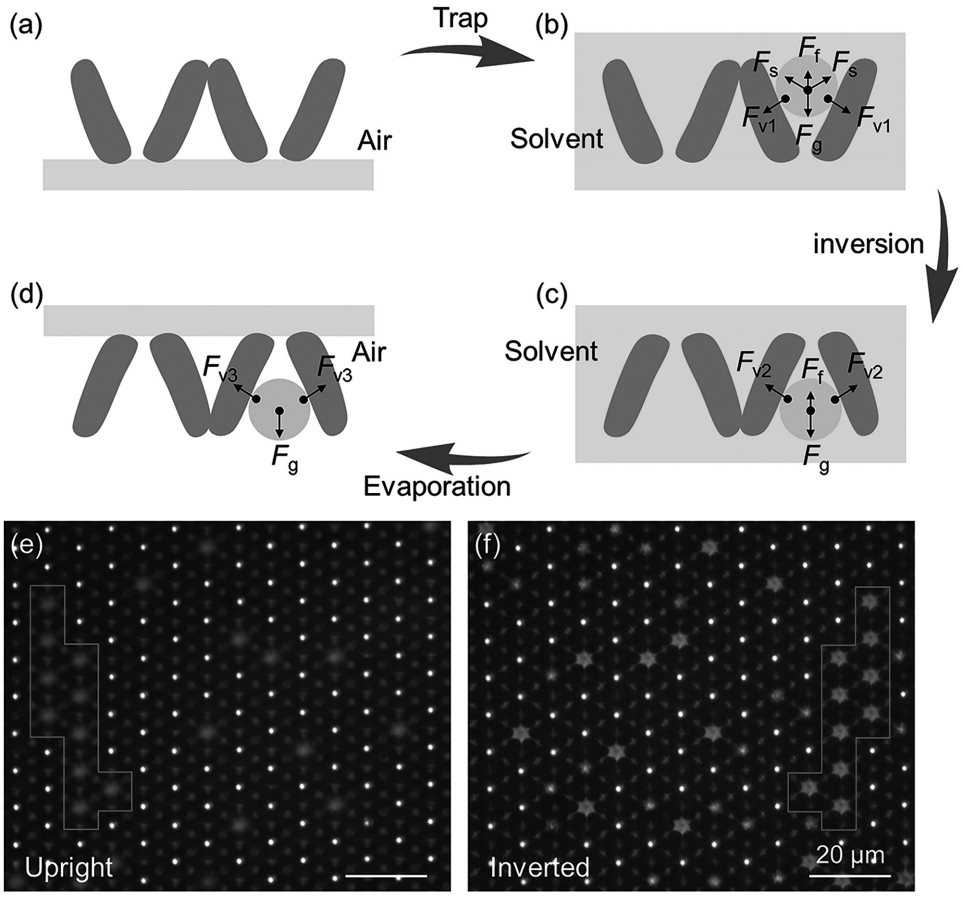

Figure 5. Schematic of the physical mechanism of the particles trapping process. a) The furcate micropillars maintain stable contact state in air. b) The SiO_2 particles are trapped stably by the balance between gravity (F_g), buoyancy (F_f), supporting force (F_s), and van der Waals force (F_{v1}). c) The van der Waals force is strong enough to maintain particles in the inverted microcavities. d) The particles are still trapped after evaporation. The optical images of e) upright and f) inverted sample with trapped particles are mirrored, indicated by the gray boxes, which also verifies the trapped particles are very stable due to the strong van der Waals force.

a 100 °C thermal platform. After polymerized by the femtosecond-laser-modulated beam, the sample was developed in 1-propanol for half an hour until all unpolymerized part is washed away. During the evaporation process after withdrawing from 1-propanol liquid, the micropillar array on the sample was induced to assemble into various complex 3D microstructures with the aid of capillary force. The femtosecond laser source is a mode-locked Ti:sapphire ultrafast oscillator (Chameleon Vision-S, from Coherent Inc, USA) with a central wavelength of 800 nm, a pulse width of 75 fs, and a repetition rate of 80 MHz. The reflective liquid-crystal SLM (Pluto NIR-2, from Holoeye Photonics AG, Germany) has 1920 × 1080 pixels, with pixel pitch of 8 μm, on which CGHs with 256 gray levels can be displayed. Only the central portion of the SLM with 1080 × 1080 pixels was used to generate the modulated beam, and the other pixels were assigned to zero as a reflective mirror. The sample was mounted on a nanopositioning stage (E545, from Physik Instrumente GmbH & Co. KG, Germany) with nanometer resolution and a 200 μm × 200 μm × 200 μm moving range to precisely locate microstructures.

Manipulation of Microspheres: SiO_2 particles with the diameter of 5 μm synthesized by Wakely Scientific Corp. Inc. were mixed in distilled water with a concentration of 10^{-3} g mL^{-1}. Because the microspheres gradually subside, the solution stored at room temperature was shaken up before use. The sample was horizontally installed on the stage of an optical microscopy. For trapping particles, the solution was dropped on the sample by a pipette until covering the assembled structures. The rest solution was blown away after 5 min with most particles sank to the bottom. In this process, a part of particles were trapped within the microcavities of assembled-pillars units. Therewith the sample was flushed by distilled water using a pipette to remove the noncaptured particles. The sample with trapped particles was turned to be vertical by a tweezer for washing ≈10 s. Then the sample is mounted on the stage for a few minutes to evaporate the rest distilled water. Finally, optical images of the sample with trapped particles in the microcavities can be caught by a CCD on the optical microscopy. This process of dropping solution with microspheres and flushing under distilled water is iterative to achieve a sample with a high trapping ratio.

Sample Characterization and Image Acquisition: The SEM images were taken with a secondary electron SEM (ZEISS EVO18) operated at an accelerating voltage of 10 keV after depositing ≈10 nm gold. An optical microscopy (CEWEI LW200-3JT/B, China) with a white light source performed imaging experiments of trapped particles. For capturing optical images of honeycomb patterns, the sample with trapped particles on the stage of optical microscope was placed, then illuminated with a white light source from below. Next, the vertical position of microscopy stage was adjusted to achieve clear images of particles foci. Finally, a mask with a letter "A" was placed on the white light source to achieve kaleidoscopic optical images.

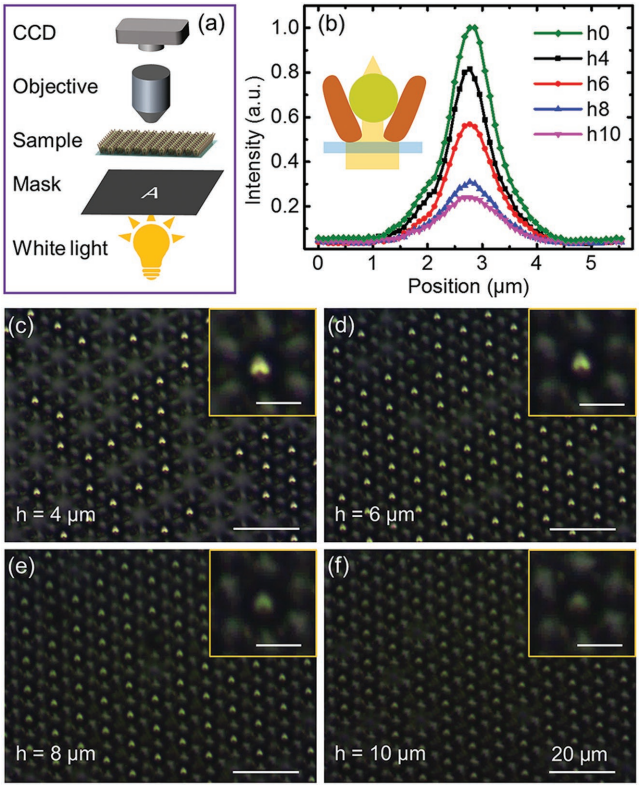

Figure 6. Imaging test of the sample after trapping SiO_2 particles. a) Schematic of optical setup for the imaging test. b) The optical intensity distributions of trapped particles foci as a function of micropillars heights. Inset is a schematic of light irradiating on a particle. c–f) Optical images of the letter "A" by the sample with varying the heights of micropillars from h = 4 to 10 μm. Insets are the magnified views of the corresponding array (scale bar, 5 μm). The 6 μm height furcate slanted micropillars have a high trapping ratio of particles, which maintain a fine imaging performance.

Supporting Information

Supporting Information is available from the Wiley Online Library or from the author.

Acknowledgements

This work was supported by National Science Foundation of China (Nos. 51275502, 61475149, 61675190, 51405464), Anhui Provincial Natural Science Foundation (No. 1408085ME104), the Fundamental Research Funds for the Central Universities (WK2480000002, WK6030000004), and "Chinese Thousand Young Talents Program."

Conflict of Interest

The authors declare no conflict of interest.

Keywords

capillary force, femtosecond lasers, microobject trapping, optical vortex, self-assembly

Received: April 12, 2017
Revised: May 18, 2017
Published online: October 16, 2017

[1] D. Wu, Q. D. Chen, H. Xia, J. Jiao, B. B. Xu, X. F. Lin, Y. Xu, H. B. Sun, *Soft Matter* **2010**, *6*, 263.
[2] C. Pang, T. I. Kim, W. G. Bae, D. Kang, S. M. Kim, K. Y. Suh, *Adv. Mater.* **2012**, *24*, 475.
[3] C. Pang, G. Y. Lee, T. I. Kim, S. M. Kim, H. N. Kim, S. H. Ahn, K. Y. Suh, *Nat. Mater.* **2012**, *11*, 795.
[4] H. G. Duan, K. K. Berggren, *Nano Lett.* **2010**, *10*, 3710.
[5] Y. L. Hu, Z. X. Lao, B. P. Cumming, D. Wu, J. W. Li, H. Y. Liang, J. R. Chu, W. H. Huang, M. Gu, *Proc. Natl. Acad. Sci. USA* **2015**, *112*, 6876.
[6] B. Pokroy, S. H. Kang, L. Mahadevan, J. Aizenberg, *Science* **2009**, *323*, 237.
[7] S. M. Kim, J. Kim, S. M. Kang, S. Jang, D. Kang, S. E. Moon, H. N. Kim, H. Yoon, *Small* **2016**, *12*, 3764.
[8] Z. X. Lao, Y. L. Hu, C. C. Zhang, L. Yang, J. W. Li, J. R. Chu, D. Wu, *ACS Nano* **2015**, *9*, 12060.
[9] D. Wu, S. Z. Wu, S. Zhao, J. Yao, J. N. Wang, Q. D. Chen, H. B. Sun, *Small* **2013**, *9*, 760.
[10] D. Chandra, S. Yang, *Acc. Chem. Res.* **2010**, *43*, 1080.
[11] J. Kato, N. Takeyasu, Y. Adachi, H. B. Sun, S. Kawata, *Appl. Phys. Lett.* **2005**, *86*, 044102.
[12] a) Y. L. Hu, Y. H. Chen, J. Q. Ma, J. W. Li, W. H. Huang, J. R. Chu, *Appl. Phys. Lett.* **2013**, *103*, 141112; b) B. Xu, W. Q. Du, J. W. Li, Y. L. Hu, L. Yang, C. C. Zhang, G. Q. Li, Z. X. Lao, J. C. Ni, J. R. Chu, D. Wu, S. L. Liu, K. Sugioka, *Sci. Rep.* **2016**, *6*, 19989; c) A. D. Wang, L. Jiang, X. W. Li, Y. Liu, X. Z. Dong, L. T. Qu, X. M. Duan, Y. F. Lu, *Adv. Mater.* **2015**, *27*, 6238.
[13] D. Wu, Q. D. Chen, B. B. Xu, J. Jiao, Y. Xu, H. Xia, H. B. Sun, *Appl. Phys. Lett.* **2009**, *95*, 091902.
[14] L. Q. Chang, D. Gallego-Perez, C. L. Chiang, P. Bertani, T. R. Kuang, Y. Sheng, F. Chen, Z. Chen, J. F. Shi, H. Yang, X. M. Huang, V. Malkoc, W. Lu, L. J. Lee, *Small* **2016**, *12*, 5971.
[15] J. E. Curtis, D. G. Grier, *Phys. Rev. Lett.* **2003**, *90*, 133901.
[16] a) J. Wang, J. Y. Yang, I. M. Fazal, N. Ahmed, Y. Yan, H. Huang, Y. X. Ren, Y. Yue, S. Dolinar, M. Tur, A. E. Willner, *Nat. Photonics* **2012**, *6*, 488; b) X. L. Cai, J. W. Wang, M. J. Strain, B. Johnson-Morris, J. B. Zhu, M. Sorel, J. L. O'Brien, M. G. Thompson, S. T. Yu, *Science* **2012**, *338*, 363.
[17] M. P. J. Lavery, F. C. Speirits, S. M. Barnett, M. J. Padgett, *Science* **2013**, *341*, 537.
[18] K. Toyoda, K. Miyamoto, N. Aoki, R. Morita, T. Omatsu, *Nano Lett.* **2012**, *12*, 3645.
[19] S. Franke-Arnold, L. Allen, M. Padgett, *Laser Photonics Rev.* **2008**, *2*, 299.
[20] a) S. Franke-Arnold, J. Leach, M. J. Padgett, V. E. Lembessis, D. Ellinas, A. J. Wright, J. M. Girkin, P. Ohberg, A. S. Arnold, *Opt. Express* **2007**, *15*, 8619; b) P. Miao, Z. F. Zhang, J. B. Sun, W. Walasik, S. Longhi, N. M. Litchinitser, L. Feng, *Science* **2016**, *353*, 464.
[21] H. Yoon, M. K. Kwak, S. M. Kim, S. H. Sung, J. Lim, H. S. Suh, K. Y. Suh, K. Char, *Small* **2011**, *7*, 3005.
[22] a) T. G. Leong, C. L. Randall, B. R. Benson, A. M. Zarafshar, D. H. Gracias, *Lab Chip* **2008**, *8*, 1621; b) T. G. Leong, C. L. Randall, B. R. Benson, N. Bassik, G. M. Stern, D. H. Gracias, *Proc. Natl. Acad. Sci. USA* **2009**, *106*, 703; c) K. Malachowski, M. Jamal, Q. R. Jin, B. Polat, C. J. Morris, D. H. Gracias, *Nano Lett.* **2014**, *14*, 4164.
[23] M. Hu, F. S. Ou, W. Wu, I. Naumov, X. M. Li, A. M. Bratkovsky, R. S. Williams, Z. Y. Li, *J. Am. Chem. Soc.* **2010**, *132*, 12820.
[24] H. R. Zhang, F. Y. Yang, J. J. Dong, L. N. Du, C. Wang, J. M. Zhang, C. F. Guo, Q. Liu, *Nat. Commun.* **2016**, *7*, 13743.
[25] M. Pisco, F. Galeotti, G. Quero, A. Iadicicco, M. Giordano, A. Cusano, *ACS Photonics* **2014**, *1*, 917.
[26] a) H. Lin, M. Gu, *Appl. Phys. Lett.* **2013**, *102*, 084103; b) X. P. Li, T. H. Lan, C. H. Tien, M. Gu, *Nat. Commun.* **2012**, *3*, 998.